voltage drop across the diode, the string voltage V_{string} is restricted to be equal to the battery voltage V_{out} at all times, which is typically not the same as the MPP voltage (V_{MPP}). For a particular operating irradiation level and temperature, the series-connected cells' V_{MPP} may coincide with V_{out}, but at all other times, less than the maximum power is extracted from the cells. Figure 4b shows a method which is typically used to circumvent this limitation. By placing a dc-dc converter between the series-connected cells and the load, the string voltage V_{string} can be controlled to equal V_{MPP} at all times. The dc-dc converter, acting as a maximum power point tracker (MPPT), continuously tracks V_{MPP} by adjusting its conversion ratio in response to changes in operating conditions.

The method of Figure 4b is often adequate for solar photovoltaic applications, where the solar irradiation is a plane-wave, ensuring uniform illumination of all cells in the series string. Provided the cells are properly matched in terms of their electrical characteristics, they will then produce equal currents. The situation is different in the TPV application considered here. Since the burner is positioned close to the TPV diode (2-3 millimeters), the irradiation is non-uniform and depends on the relative position of the diode with respect to the burner. In addition, the temperature distribution across the burner surface is non-uniform. This leads to mismatched cell photocurrents, with the cell receiving the most irradiation producing the most current. If a method similar to that of Figure 4b is employed in this situation, the string current I_{string} is limited to the value of the least irradiated cell. Thus, all other cells are operating at a cell current that is below their peak current, resulting in a total output power that can be substantially lower than the maximum achievable. The result is similar to that observed in solar panels with partial shading, as discussed in [7], [8]. The non-uniform irradiation in this application prevents efficient energy extraction with the stacking of many cells in series to achieve a high output voltage.

Figure 4c shows the architecture we propose to ameliorate these concerns. In this architecture, four diodes are connected in series and form a module. Each module is then connected to its own individual MPPT, and the outputs of all MPPTs are connected in parallel. The choice of four cells per module was made to provide a large enough working voltage (approximately 1 V) for the MPPTs to ensure efficient power conversion by the electronics. Using this architecture, current mismatch is limited to only four cells, all of which are placed in close proximity to each other, thereby minimizing the negative effects of non-uniform irradiation. The boxed area of Figure 4c highlights the system components that are considered in this work, which constitute four series-connected cells and one MPPT.

III. Peak Power Tracking Implementation

Figure 5 shows a schematic drawing of the implementation of one of the MPPTs of Figure 4c. The low-voltage PV module (with the I-V characteristics of Figure 3) is used to charge a lithium-ion battery, which acts as intermediate energy storage for the system. The power electronic circuit is implemented as a boost converter, which performs both the requisite voltage transformation and the peak power tracking.

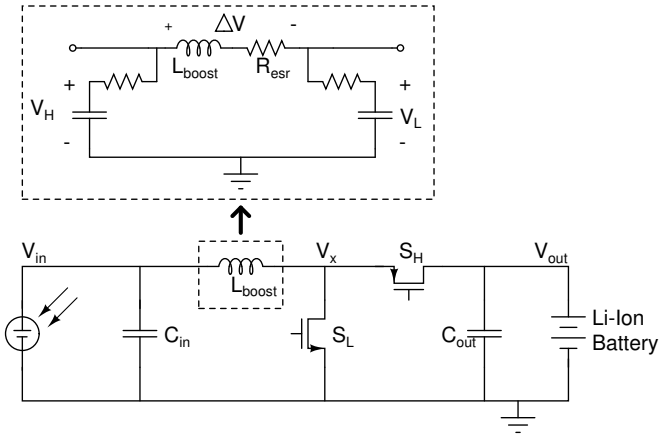

Fig. 5. Schematic drawing of MPPT, and an illustration of the lossless current sensing scheme used.

A. Control Algorithm and Implementation

The boost converter shown in Figure 5 has an input/output voltage relationship given by:

$$V_{out} = \frac{V_{in}}{1 - D} \tag{1}$$

where D is the duty cycle of the bottom switch (S_L). In this synchronous rectification implementation, the top switch (S_H) is turned on when the bottom switch is off. The boost converter can be controlled to achieve peak power tracking by perturbing the duty cycle in a certain direction (increase or decrease), and observe whether the delivered power increased or decreased due to this perturbation. If the power increased, the controller continues to perturb the duty cycle in the same direction, but if the power decreased, the direction of the perturbation is changed. With this method, the controller eventually settles on the peak power point of Figure 3, where it oscillates to within the finest resolutions of the duty cycle command and sensors. This method, often called hill climbing, or perturb and observe, [9] is one of the most common MPPT algorithms used to date. Figure 6 shows a flow chart of the MPPT algorithm. The initial starting point for the duty cycle is determined by performing a coarse sweep of the duty cycle at startup, and recording the duty cycle corresponding to the maximum output power observed. This approach ensures that peak power tracker can quickly lock in on the maximum power point.

The algorithm described above is well-suited for an implementation in digital form, and we have chosen to use a microcontroller for our implementation. In addition to keeping state and running the tracking algorithm, the microcontroller can be used to perform analog to digital conversion, generate the PWM signals, perform temperature measurements, and handle communication. The ability of the microcontroller to handle a variety of functions is very beneficial in this low-power application, where the power loss of the auxiliary components must be kept to a minimum. An additional benefit

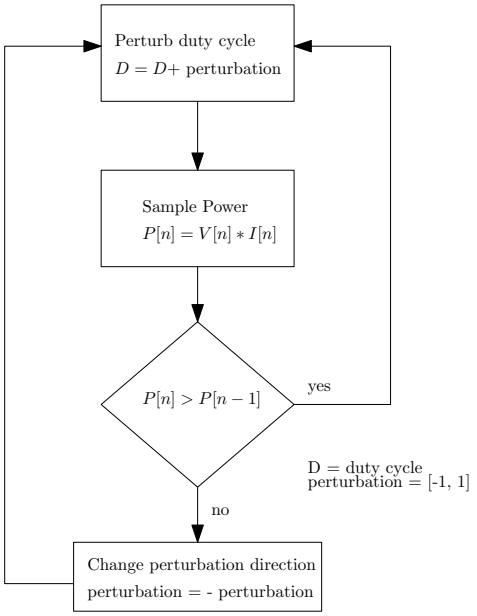

Fig. 6. Flow chart illustrating the operation of perturb and observe .

of a multi-function chip such as the micro-controller is the significant space savings that can be realized compared to an implementation with discrete devices for each function.

B. Voltage and Current Measurement

In the general case, both current and voltage must be measured to find the maximum power point (see [7] for a discussion of cases where only one of the two needs to be measured). Typically, only the average values need to be measured, which reduces bandwidth requirements and enables the use of low-power analog to digital converter (ADC) architectures. Furthermore, the absolute value of current and voltage is not required, since the minimum or maximum power points are found relative to the other possible operating points. The ADC thus needs high resolution, but not high absolute precision, a characteristic that can be leveraged to obtain high performance while maintaining low power consumption.

The microcontroller used, the 8-bit ATtiny861 from Atmel, provides a multiplexed 10-bit ADC, along with an internal bandgap reference. The 10-bit precision can be further extended in the digital domain by oversampling and decimation [10]. The input and output voltages can thus easily be measured with this built-in ADC with sufficient resolution.

A more difficult challenge is that of current sensing, which is typically done with a current-sense resistor. The addition of a current-sense resistor in the current path introduces an undesired power loss, which decreases overall converter efficiency. For this reason, the current-sense resistor is typically made small, and the subsequently small voltage drop is sensed with a low-noise, high gain amplifier. In this application, with a total output power of less than 500 mW, the additional power consumption and area of a low-noise amplifier for current sensing, together with the added power loss of a current-sense resistor, was deemed too high, so alternative implementations were investigated.

Another current-sensing option is that of a hall-effect sensor, which measures the magnetic field associated with a current. With no added resistor in the current path, the only power loss is that of the magnetic sensing circuitry, which can unfortunately be quite large. Indeed, in this application it was found that the static power consumption of this method was much too large for acceptable system efficiency.

Figure 5 illustrates the current-sensing technique used in the power tracker. To maximize overall system efficiency, lossless current sensing [11] is used, where the average voltage drop across the inductor is measured. The relationship between inductor current I_L and sensed voltage ΔV is given by:

$$\langle I_L \rangle R_{esr} = \langle \Delta V \rangle = \langle V_H \rangle - \langle V_L \rangle, \tag{2}$$

where R_{esr} is the parasitic resistance of the inductor. The average voltages, $\langle V_H \rangle$ and $\langle V_L \rangle$ are produced by first-order RC low-pass filters. These two voltages are then sampled by the differential ADC of the micro-controller with a built-in gain of 32, which gives a reading directly proportional to the inductor current. It should be noted that the common concern with this current sensing method, the tolerance and temperature coefficient of R_{esr}, is not a problem in this application. Since, for our tracking algorithm, we are only concerned with relative changes of the current, any static offset of R_{esr} has no effect on the peak power tracking. Furthermore, the time constant of any temperature-induced variation of the R_{esr} value is much larger than the chosen sampling time, so the tracking can be made insensitive to this variation as well. In our converter implementation, a relative change in current of less than 1 mA can be resolved using this method, as confirmed by experimental measurements. It should be noted that this current sensing is achieved without the need for a power-consuming series-sense resistors, and that the amplifier and ADC are built-in to the microcontroller, and thus consume negligible additional power and take up no additional area.

It should be emphasized that a key enabler to the use of this current-sensing technique is the fact that the application does neither require absolute accuracy of the current, nor instantaneous current values. Thus, the tolerance of the inductor resistance is not critical, and the low-pass filters can be designed to provide significant averaging over a relatively long time.

IV. Prototype and Experimental Results

A. Converter prototype

An experimental prototype of the MPPT converter has been developed and characterized. Figure 7 shows a photograph of the peak power tracker, and Table I lists the converter specifications; converter efficiency includes all control and gate driver losses. The tracking efficiency is a measurement of how close the tracking algorithm operates to the true maximum power point, and is given by:

$$\eta_{tracking} = \frac{\langle P_{in} \rangle}{P_{MPP}}, \tag{3}$$

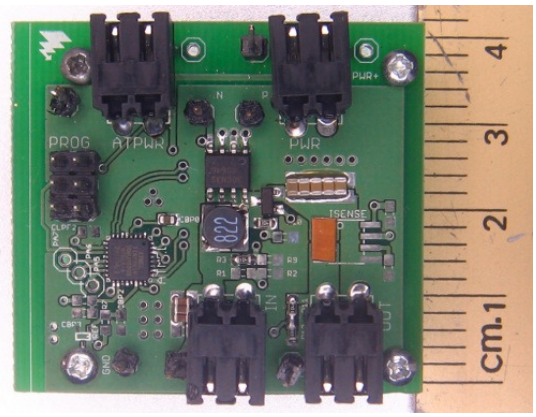

Fig. 7. Photograph of the peak power tracker.

where P_{in} corresponds to the converter input power, and P_{MPP} is the output power of the TPV module at the maximum power point. Due to the low operating point of the TPV module ($\sim$ 1 V), it is difficult to make a high precision input power measurement of the converter without also perturbing the actual operating point of the converter. An easier, but strictly speaking less accurate, approximation of the tracking efficiency can be found by calculating the ratio:

$$\eta_{tracking,approx.} = \frac{\langle P_{out} \rangle}{P_{out,max}}, \tag{4}$$

where $P_{out,max}$ corresponds to the maximum output power from the converter. This is only an approximation, and will over-estimate the tracking efficiency because $P_{out,max}$ will not correspond to the exact peak power point, owing to the finite resolution of the digital PWM implementation. However, with proper knowledge of the cell I-V curve (Figure 3) and the tracking algorithm step-size (PWM resolution is this implementation), one can find an upper bound on the error in the approximation given by 4, and from there calculate a minimum tracking efficiency. Using this technique, the tracking efficiency of the converter considered here was found to be above 99%.

The converter design was guided by the desire to achieve small system size and weight, while maintaining high efficiency. As can be seen in Figure 7, the majority of the circuit board area is taken up by connectors, while the converter core (switching devices, micro-controller, and passive components) take up a relatively small area. Figure 8 provides a detailed schematic drawing of the converter. As shown, the converter can be powered either from the Li-Ion battery output, or from an external power supply. Table II lists the components used in the experimental prototype.

B. Converter experimental verification

To evaluate the performance of the peak power tracker, the converter was initially connected to a PV diode illuminated by a quartz halogen lamp. The lamp brightness and distance from the cell was adjusted to match the expected power output from the cell when illuminated by the micro-reactor (500 mW).

TABLE I
CONVERTER SPECIFICATIONS

Input Voltage	0.3-1.1 V
Output Voltage	1.5-4.2 V
Output Power	500 mW
Switching Frequency	250 kHz
Converter Efficiency	90%
Tracking Efficiency	>99%

TABLE II
COMPONENT LISTING

Device	Model	Value	Manufacturer
S_1	BSO300N03S		Infineon Tech.
S_2	SI2351DS		Vishay Siliconix
L	MSS5131-822ML	8.2 μH	Coilcraft
R_H, R_L	0603	100 kΩ	Panasonic
C_H, C_L	0603	10 μF	Murata
C_{IN}	0805	3 μF	Murata
C_{OUT}	0805	50 μF	Murata
Microcontroller	ATtiny861		Atmel
Gate Driver	LM5111		National Semi.

This enabled initial characterization of the converter without the added complexity of the micro-reactor dynamics. Figure 9 (top) shows the output power of the converter over time, and illustrates the MPPT startup algorithm for this experimental setup. Initially, the converter steps its duty cycle through a coarse sweep to find the approximate point of the MPP. The duty cycle corresponding to the maximum power observed is recorded, and once the sweep is concluded, the duty cycle is set to this value. At this point, the converter enters the hill-climbing phase (perturb and observe), and uses a fine step-size to reach the MPP. Note that the step-size of the hill-climbing algorithm is too small to be visible in the top plot.

The steady-state behavior of the hill-climbing algorithm is shown in the bottom of the figure, which shows the converter output power versus time in steady-state. This is a zoomed-in version of the top plot, and shows the discrete steps in power corresponding to a 1-bit change in duty cycle. The total PWM resolution of the micro-controller is 10 bits. The converter oscillates around the MPP to within the resolution of the PWM signal and the current and voltage sensors. Because the sensing and duty cycle control have similar resolution, the hill-climbing algorithm is limited by sensing noise, and occasionally takes one extra step in the wrong direction. It should be noted that the sampling interval for the MPPT algorithm has been set to several seconds, as seen in Figure 9 (bottom). This was done to enable high accuracy power measurements by the external instruments used to characterize the converter, and is not a fundamental limit of the converter itself. If desired, the MPPT algorithm can be set to sampling frequencies considerably higher (on the order of several kHz) without a noticeable impact on tracking efficiency. In this application, however, the system time constant of any change in maximum power point is long enough such that the sampling frequency of Figure 9 is sufficient to allow efficient energy extraction from the PV

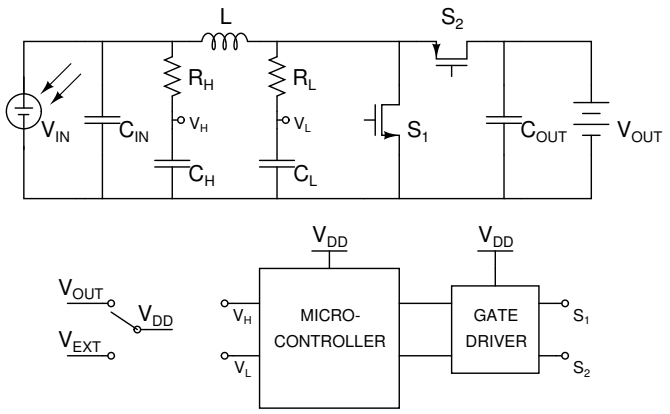

Fig. 8. Schematic drawing of converter.

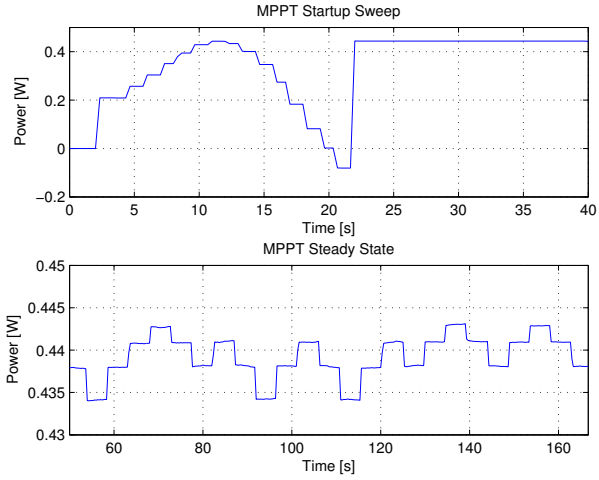

Fig. 9. Experimental data showing startup behavior of power tracker (top), and steady-state performance (bottom).

module.

C. Micro-reactor experimental results

In order to fully evaluate the MPPT converter performance we tested it with an experimental system setup similar to the one depicted in Figure 2. The PV cells were illuminated with the micro-reactor, shown in the photo of Figure 10. The reactor is a 10 mm by 10 mm by 1 mm silicon slab with a serpentine, platinum catalyst-loaded channel running through it [5]. A mixture of butane and oxygen is fed into one end of the channel; carbon dioxide and water vapor are exhausted from the other end. With a butane flow of 8 sccm (standard cubic centimeters per minute) and 80 sccm of oxygen, the average surface temperature is 850°C. For reference, an ordinary pocket lighter burns 15 sccm of butane.

In the experimental setup, the two GaInAsSb PV cells are located directly above the burner and another two cells are located below the burner as shown in Figure 10. These four PV cells are connected in series and their output is connected to the MPPT converter. Experimental data from the complete system setup is shown in Figure 11, which shows converter

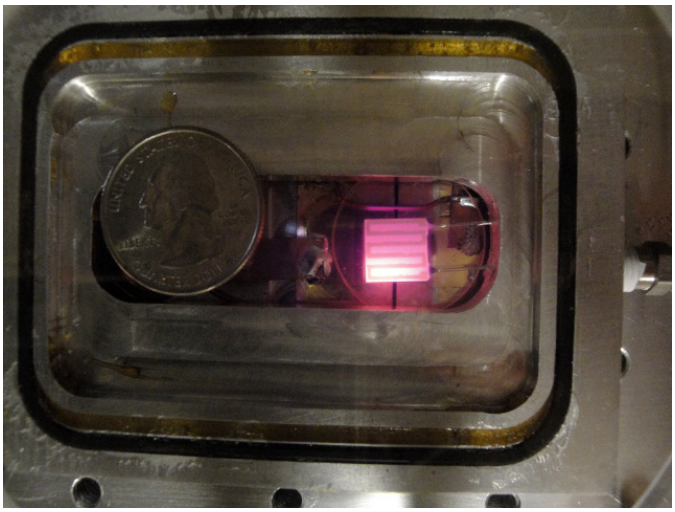

Fig. 10. Photograph of the experimental setup with the top two PV cells removed and a US quarter for scale. The MEMS burner and the bottom two PV cells are visible.

output power versus time. As expected, this plot looks similar to Figure 9, but there are some notable differences. This first generation micro-reactor assembly has a typical output power of 150 mW, due to the cell being placed at a distance from the burner that is too far for optimum power transfer. Despite this, the demonstrated system output power is more than two orders of magnitude higher than what has previously been achieved [12]. The measured energy density of this micro-TPV system is 75 mW/cm^2. For comparison, the best power densities reported for micro scale direct methanol fuel cell (DMFC), with comparable size to this TPV system, are in the range from 4 to 30 mW/cm^2 [13]. It should be noted that while this early burner prototype has a lower efficiency than the fuel cell presented in [13], previous TPV results [4] show that a comparable efficiency to that of a fuel cell system is achievable. With better system packaging and by further optimizing the system design we are targeting a micro-TPV system power density of 250-300 mW/cm^2.

One of the difficulties encountered during system testing was that the burner experiences occasional temperature fluctuations due to condensed butane entering the fuel supply. Butane is delivered to the burner as a gas but occasional droplets, representing additional fuel, can enter the inlet stream. When a droplet enters the burner, there is a sudden increase in temperature as it burns. Figure 11 captures such an event, which occurs slightly before time t=45 seconds, with a correspondingly large increase in output power, followed by an exponential decay back to steady-state. The time constant associated with this event is such that the MPPT algorithm may take one or two steps in the wrong direction during the increasing power phase, followed by a continuous change of direction during the exponential decay, since the output power at each sample time is lower than the previous sample. The result is that while the converter may operate slightly off of the peak power point during this transient event, it is guaranteed

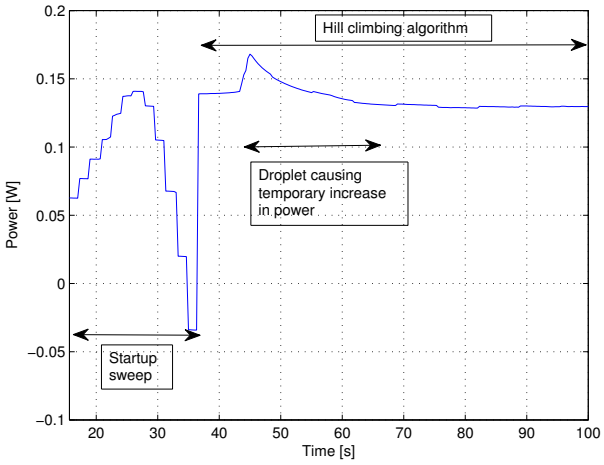

Fig. 11. Experimental data showing the output power of the MPPT as a function of time. The temporary increase in output power around time t=45 seconds is due to a butane droplet forming and causing an increase in burner temperature.

not to move more than a few steps in the wrong direction, ensuring a quick return to the maximum power point once the burner has returned to equilibrium.

V. Conclusion

We have demonstrated a power electronics architecture suitable for TPV power generation. The proposed architecture addresses challenges that are unique to the TPV application, and enables a substantial increase in energy capture compared to conventional methods. We incorporate low-power sensing techniques and achieve high power conversion efficiency and small size. A tracking efficiency above above 99% is demonstrated. In addition, we have demonstrated a micro-TPV system generating 150 mW with the MPPT converter. These results pave the way towards a fully integrated, fully functional micro-scale TPV power generator.

References

[1] H. Kolm, "Solar-battery power source," quarterly progress report, solid state research, group 35, MIT-Lincoln laboratory, 1956.

[2] I. Celanovic, N. Jovanovic, and J. Kassakian, "Two-dimensional tungsten photonic crystals as selective thermal emitters," *Applied Physics Letters*, vol. 92, pp. 193101–+, May 2008.

[3] I. Celanovic, F. O'Sullivan, M. Ilak, J. Kassakian, and D. Perreault, "Design and optimization of one-dimensional photonic crystals for thermophotovoltaic applications," *Optics Letters*, vol. 29, p. 863, 2004.

[4] B. Wernsman, R. Siergiej, S. Link, R. Mahorter, M. Palmisiano, R. Wehrer, R. Schultz, G. Schmuck, R. Messham, S. Murray, C. Murray, F. Newman, D. Taylor, D. DePoy, and T. Rahmlow, "Greater than 20 percent radiant heat conversion efficiency of a thermophotovoltaic radiator/module system using reflective spectral control," *IEEE Transactions on Electron Devices*, vol. 51, no. 3, pp. 512– 515, 2004.

[5] B. Blackwell, *Design, fabrication, and characterization of a micro fuel processor*. PhD thesis, Massachusetts Institute of Technology, 2008.

[6] M. W. Dashiell, J. F. Beausang, H. Ehsani, G. J. Nichols, D. M. Depoy, L. R. Danielson, P. Talamo, K. D. Rahner, E. J. Brown, S. R. Burger, P. M. Fourspring, W. F. TopperJr., P. F. Baldasaro, C. A. Wang, R. K. Huang, M. K. Connors, G. W. Turner, Z. A. Shellenbarger, G. Taylor, J. Li, R. Martinelli, D. Donetski, S. Anikeev, G. L. Belenky, and S. Luryi, "Quaternary InGaAsSb thermophotovoltaic diodes," *IEEE Transactions on Electron Devices*, vol. 53, pp. 2879–2891, Dec. 2006.

[7] C. Sullivan and M. Powers, "A high-efficiency maximum power point tracker for photovoltaic arrays in a solar-powered race vehicle," in *Proc. 24th Annual IEEE Power Electronics Specialists Conference PESC '93 Record*, pp. 574–580, 1993.

[8] A. Woyte, J. Nijs, and R. Belmans, "Partial shadowing of photovoltaic arrays with different system configurations: literature review and field test results.," *Solar Energy*, vol. 74, pp. 217–233, 2003.

[9] T. Esram and P. Chapman, "Comparison of photovoltaic array maximum power point tracking techniques," *IEEE Transaction on Energy Conversion*, vol. 22, no. 2, pp. 439–449, 2007.

[10] Atmel, "AVR121: Enhancing ADC resolution by oversampling," application note, 2005.

[11] X. Zhou, P. Xu, and F. Lee, "A novel current-sharing control technique for low-voltage high-current voltage regulator module applications," *IEEE Transactions on Power Electronics*, vol. 15, no. 6, pp. 1153–1162, 2000.

[12] O. Nielsen, L. Arana, C. Baertsch, K. Jensen, and M. Schmidt, "A thermophotovoltaic micro-generator for portable power applications," in *TRANSDUCERS, Solid-State Sensors, Actuators and Microsystems, 12th International Conference on, 2003*, vol. 1, pp. 714–717 vol.1, June 2003.

[13] A. Kamitani, S. Morishita, H. Kotaki, and S. Arscott, "Miniaturized microdmfc using silicon microsystems techniques: performances at low fuel flow rates," *J. Micromech. Microeng.*, vol. 18, p. 125019, 2008.